Numerical Investigation into the Performance of Two Reconfigurable Gaseous Plasma Antennas

D. Melazzi[1], V. Lancellotti[2], P. De Carlo[3], M. Manente[4], D. Pavarin[3], T. Anderson[5]
[1]University of Padova, CISAS "G.Colombo", Padova, Italy, davide.melazzi@gmail.com
[2]Faculty of Electrical Engineering, Eindhoven University of Technology,
Eindhoven, The Netherlands, v.lancellotti@tue.nl
[3]University of Padova, Department of Industrial Engineering, Padova, Italy
[4]hit09 S.r.l, Padova, Italy
[5]Haleakala Research and Development Inc., Brookfield, MA, USA

***Abstract*—Plasma antennas constitute a promising alternative to conventional metallic antennas for applications in which reconfigurability with respect to some property is desired. The latter feature can be achieved by tuning the plasma discharge parameters. We use a full-wave numerical tool, ADAMANT (Advanced coDe for Anisotropic Media and ANTennas), based on integral equations, to assess the role played by plasma discharge parameters in shaping the radiation pattern, which is mainly determined by the plasma current distribution. Numerical results for different discharge parameters show that the antenna radiation efficiency can be controlled by adjusting plasma density and magneto-static field.**

I. Introduction

Gaseous Plasma Antennas (GPAs) are devices that rely on a partially or fully ionized gas (rather than just metallic parts) to radiate electromagnetic (EM) waves [1]. That is why GPAs have potential advantages over conventional metallic antennas: (i) GPAs are reconfigurable with respect to input impedance, radiation pattern, frequency of operation and bandwidth; (ii) they can be reconfigured electrically — rather than mechanically — on time scales the order of microseconds to milliseconds; (iii) they have lower thermal noise and minimal signal degradation, because they are energized only while the communication takes place; (iv) they are virtually "transparent" above the plasma frequency and become "invisible" once turned off; (v) they have lower side lobes. Last but not least, GPAs operating at different frequencies do not interfere with each other — which enables, e.g., stacking arrays of antennas. Besides, the influence of an external magnetizing field has not been fully understood yet, and the presence of the latter seems to provide: (i) enhanced plasma conductivity thanks to an efficient and high-density plasma production; (ii) a truly 3-D plasma current distributed throughout the volume; and (iii) ability to change the plasma current, thus giving full control on the GPA properties.

So far GPAs have been analyzed with simplified numerical approaches [2], [3] based on an *isotropic* (i.e., non-magnetized) plasma model. Therefore, the accurate analysis and design of highly reconfigurable GPAs must necessarily account for a tensor plasma permittivity $\overline{\varepsilon}$ which is possibly function of plasma discharge parameters along with the static magnetic field that makes the plasma a gyrotropic medium.

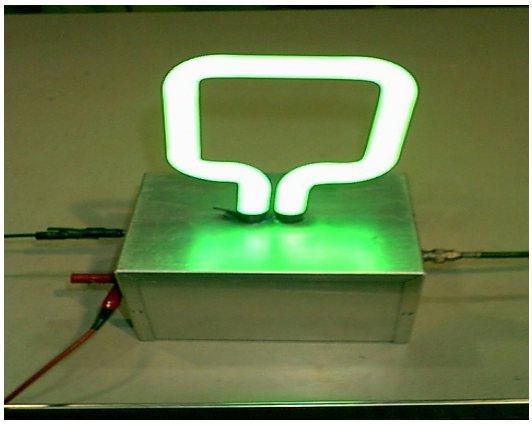

Fig. 1: Example of basic plasma antenna.

To assess the role of the plasma discharge parameters in the radiation efficiency of a plasma antenna, we use ADAMANT (Advanced coDe for Anisotropic Media and ANTennas), which features a full-wave approach based on the numerical solution of coupled surface and volume integral equations. This strategy allows determining an accurate plasma response in terms of 3-D current distribution, from which the radiation pattern can be computed. Likewise, the input impedance of the GPA can be derived and used to design the matching network.

In what follows we briefly outline the formulation and the numerical solution of the EM problem, as implemented in ADAMANT. Finally, we present results in terms of antenna input impedance and radiation pattern for GPAs of different shape and for various working conditions of the plasma discharge.

A time dependence in the form $\exp(\mathrm{j}\omega t)$ for fields and sources is assumed and suppressed throughout.

II. The ADAMANT numerical code

We formulate an EM problem such as the one in Fig. 1 by applying the Volume and the Surface Equivalence Principle. The former requires introducing a set of volume polarization

currents

$$\begin{aligned}\mathbf{J}_{Pk}(\mathbf{r}) &= \mathrm{j}\omega[\overline{\mathbf{I}} - \overline{\varepsilon}_{rk}^{-1}(\mathbf{r})] \cdot \mathbf{D}_{Pk}(\mathbf{r}) \\ &= \mathrm{j}\omega\overline{\boldsymbol{\alpha}}_k(\mathbf{r}) \cdot \mathbf{D}_{Pk}(\mathbf{r}),\end{aligned} \tag{1}$$

for $k = 1, \ldots, N_P$, with N_P being the number of independent plasma columns that forms the GPA and $\mathbf{D}_{Pk}$ the total displacement vector within the kth plasma region. The tensors $\overline{\varepsilon}_{rk}$ denote the plasma permittivities relative to vacuum. In a GPA, the plasma is cold, and weakly collisional. Additionally, if present, a static magnetic field $\mathbf{B_0}$ is assumed to be aligned with the $\hat{\mathbf{z}}$ axis in a system of Cartesian coordinates. The dielectric tensor $\overline{\varepsilon}_{rk}$ reads:

$$\overline{\varepsilon}_r = \begin{bmatrix} S & jD & 0 \\ -jD & S & 0 \\ 0 & 0 & P \end{bmatrix}, \tag{2}$$

where

$$S = 1 - \sum_{\xi} \frac{\omega_{p\xi}^2(\omega - j\nu_\xi)}{\omega[(\omega - j\nu_\xi)^2 - \omega_{c\xi}^2]} \tag{3}$$

$$D = \sum_{\xi} \frac{\sigma_\xi \omega_{c\xi}}{\omega} \frac{\omega_{p\xi}^2}{\left[(\omega - j\nu_\xi)^2 - \omega_{c\xi}^2\right]} \tag{4}$$

$$P = 1 - \sum_{\xi} \frac{\omega_{p\xi}^2}{\omega\,(\omega - j\nu_\xi)} \tag{5}$$

with the plasma frequency $\omega_{p\xi} \equiv (n_\xi q_\xi^2/\varepsilon_0 m_\xi)^{1/2}$, the gyrofrequency $\omega_{c\xi} \equiv \sigma_\xi q_\xi B_0/m_\xi$ with σ_ξ the particle charge sign, the collision frequency ν_ξ. The subscript ξ refers to the index of the plasma species. Moreover, in writing (1) we assume $\overline{\varepsilon}_{rk}$ to be a function of the position. Therefore, profiles of plasma density, magnetic field, electron temperature, and neutral pressure can be included.

We apply the Surface Equivalence Principle to the metallic parts S_A which, as a result, are replaced with an unknown electric surface current density $\mathbf{J}_A$. By enforcing the relevant boundary conditions on the conducting surface S_A and expressing the total electric field in the N_P regions occupied by plasma we arrive at the set of coupled surface and volume integral equations

$$\begin{aligned}\mathbf{E}_A^{\mathrm{i}}(\mathbf{r}) + \omega^2\mu_0\overline{\mathbf{G}}(\mathbf{r}) \overset{*}{\cdot} \left[\sum_{k=1}^{N_P} \overline{\boldsymbol{\alpha}}_k(\mathbf{r}) \cdot \mathbf{D}_{Pk}(\mathbf{r})\right] \\ -\mathrm{j}\omega\mu_0\overline{\mathbf{G}}(\mathbf{r}) \overset{*}{\cdot} \mathbf{J}_A(\mathbf{r})\Big|_{\tan} = 0, \quad \mathbf{r} \in S_A,\end{aligned} \tag{6}$$

$$\begin{aligned}\overline{\varepsilon}_r^{-1} \cdot \mathbf{D}_{Pk}(\mathbf{r}) = -\mathrm{j}\omega\varepsilon_0\mu_0\overline{\mathbf{G}}(\mathbf{r}) \overset{*}{\cdot} \mathbf{J}_A(\mathbf{r}) \\ + k_0^2\,\overline{\mathbf{G}}(\mathbf{r}) \overset{*}{\cdot} \left[\sum_{l=1}^{N_P} \overline{\boldsymbol{\alpha}}_l(\mathbf{r}) \cdot \mathbf{D}_{Pl}(\mathbf{r})\right], \quad \mathbf{r} \in V_{Pk},\end{aligned} \tag{7}$$

where $\overline{\mathbf{G}}(\mathbf{r})$ is the dyadic Green's function in free space and '$\overset{*}{\cdot}$' signifies 3-D spatial convolution and scalar product. Finally, $\mathbf{E}_A^{\mathrm{i}}$ is the impressed electric field at the antenna port in the voltage-gap approximation.

We solve the system (6), (7) of $N_P + 1$ equations numerically by means of the Method of Moments in the form of Galerkin. To this end, we model the conductors with a 3-D triangular-faceted mesh and the plasma with a tetrahedral mesh. Then, we associate surface (volume) div-conforming vector linear elements $\mathbf{f}(\mathbf{r})$ ($\mathbf{v}(\mathbf{r})$) with the inner edges (all the facets) of the triangular (tetrahedral) mesh, in order to expand $\mathbf{J}_A$ ($\mathbf{D}_{Pk}$).

We mention in passing that the algebraic system that arises from the testing procedure applied to (6), (7) is not symmetric. The lack of symmetry, though, is not merely a consequence of the plasma being gyrotropic (i.e., non-reciprocal). In fact, the system matrix would not be symmetric, even if the tensors (2) happened to be so, because $\overline{\mathbf{G}}$ and $\overline{\boldsymbol{\alpha}}_k$ in (6), (7) do not commute in general. In that case, as it turns out, overall symmetry could be gained, if the volume test functions for (7) were chosen to be $[\overline{\boldsymbol{\alpha}}_{rk}(\mathbf{r}) \cdot \mathbf{v}(\mathbf{r})]^T$ at the cost of little additional complexity in the evaluation of the integrals.

From the knowledge of $\mathbf{J}_A$ the input impedance of the GPA can be derived to design the matching network, while from $\mathbf{J}_{Pk}$ the radiation pattern can be evaluated. The simulation strategy based on equations (6), (7) together with the MoM solution has been implemented in ADAMANT [4].

III. Results

We consider two GPAs with different gemetrical configurations, as shown in Fig. 2. In Fig. 2a, a cylindrical plasma column, hereinafter referred to as *plasma dipole*, is suspended above a finite ground plane, and a metallic sleeve (placed at the bottom of the plasma cylinder) is used to drive the plasma discharge. Besides, the plasma is magnetized by an external magneto-static field $\mathbf{B_0}$ parallel to the axis of the cylinder. The length of the plasma column is 60 cm, and its radius is 1 cm. The metal sleeve is 2 cm high and its radius is 1.4 cm. The metal ground below the plasma column is 25.2 cm by 3.2 cm. The operating frequency of interest is $f = 125$ MHz, so the electric length of the plasma antenna above the metal ground is approximately $\lambda_0/4$, where λ_0 is the free-space wavelength. In Fig. 2b, a similar metallic sleve is placed at the bottom of a toroidal plasma discharge. This configuration, hereinafter

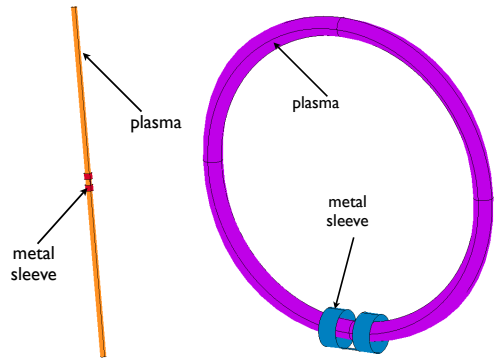

Fig. 2: GPAs: (a) plasma dipole; (b) plasma torus.

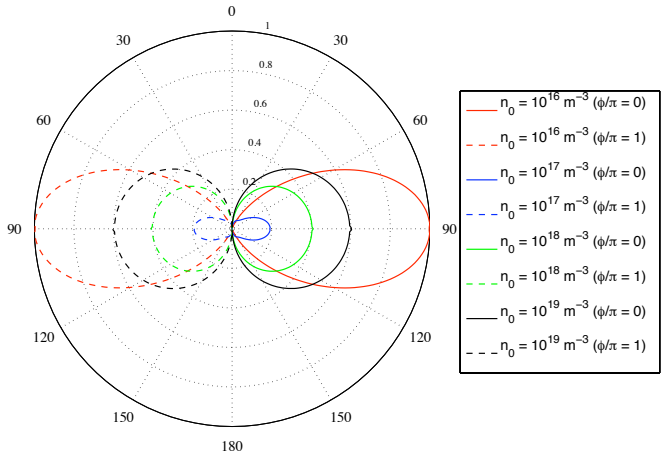

Fig. 3: Radiation pattern of the GPA in Fig. 2a for a magnetized ($\mathbf{B_0} = 50$ mT) plasma driven at $f = 125$ MHz, for different values of the plasma density (n_0).

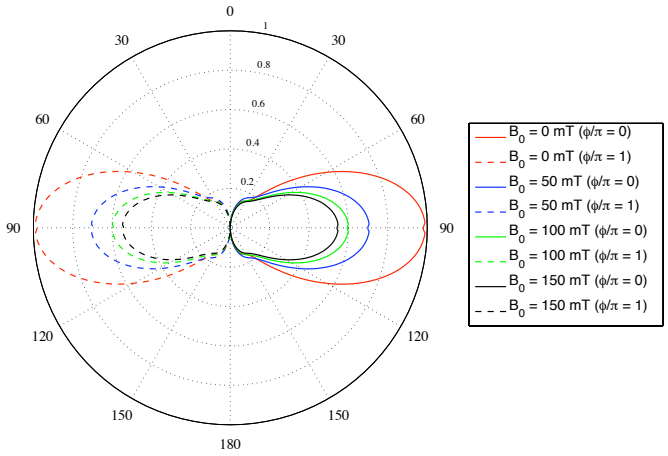

Fig. 4: Radiation pattern of the GPA in Fig. 2a for a uniform plasma driven at $f = 125$ MHz, with density $n_0 = 10^{17}$ m^{-3} for different values of the magneto-static field ($\mathbf{B_0}$).

referred to as *plasma torus*, has a minor radius $r = 1$ cm, and a major radius $R \approx 16$ cm; the operating frequency is $f = 300$ MHz, so that the plasma torus is approximately λ_0. In this last case the plasma is non-magnetized.

A. Plasma Dipole

In order to investigate the influence of plasma discharge parameters on the performance of the dipole GPA, we have considered an Argon plasma with: (i) the magneto-static field $\mathbf{B_0}$ in the range $0 - 150$ mT, (ii) the plasma density n_0 in the range $10^{16} - 10^{19}$ m^{-3}. We assume a neutral background pressure of 15 mTorr, for a weakly ionized plasma with an electron temperature of 3 eV. In the numerical solution of (6), (7), ~ 10000 and ~ 1000 linear div-conforming vector elements have been used in the plasma volume and on the metal parts, respectively.

We have computed the radiation pattern (RP) as a function of the plasma density and the external magnetic field. The results are drawn in linear scale for ease of comparison, and we have normalized the RPs to the absolute maximal value.

From Fig. 3 it is evident that the radiation pattern can be controlled by adjusting the plasma density, when the confinement magneto-static field inside the discharge of the GPA is given. Radiation patterns for different values of $\mathbf{B_0}$ are similar in shape, while the intensity of the radiated field can be controlled with the magneto-static field. As expected, the RP resembles that of a metallic $\lambda_0/4$ dipole antenna when the plasma density is high enough ($n_0 > 10^{18}$ m^{-3}).

The role played by the static magnetic field is even more evident in Figs. 4, 5, for two different plasma density values $n_0 = 10^{17}$ m^{-3} and $n_0 = 10^{19}$ m^{-3}, respectively. As mentioned above, the shape of the radiation pattern is somewhat insensitive to $\mathbf{B_0}$. However, the value of the magneto-static field can be used to control the field intensity at low plasma density (e.g., Fig. 4), but its influence becomes negligible as the plasma density increases (e.g., Fig. 5).

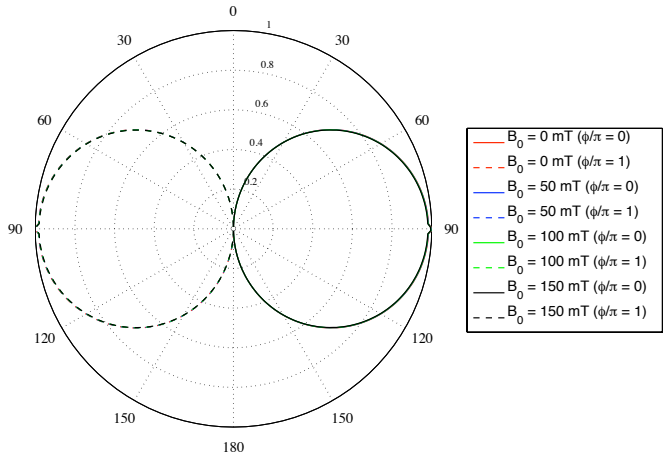

Fig. 5: Radiation pattern of the GPA in Fig. 2a for a uniform plasma driven at $f = 125$ MHz, with density $n_0 = 10^{19}$ m^{-3} for different values of the magneto-static field ($\mathbf{B_0}$).

As regards the GPA behavior as a circuit element, in Figs. 6, 7, we have plotted the real and imaginary part of the input impedance, respectively, as a function of the uniform plasma density for different external magnetic fields ($\mathbf{B_0}$), in order to investigate the combined effect of $\mathbf{B_0}$ and n_0. Simulation results indicate that the real part decreases if the magnetizing field does so (Fig. 6), whereas the imaginary part does not have a univocal trend.

B. Plasma Torus

We have considered an Argon plasma discharge with a neutral background pressure of 15 mTorr and an electron temperature of 3 eV. In order to investigate the influence of plasma discharge parameters on the performance of the plasma torus, we have computed the radiation pattern and the input impedance as a function of the plasma density n_0 in the range $10^{16} - 10^{19}$ m^{-3}. We assume a uniform plasma density

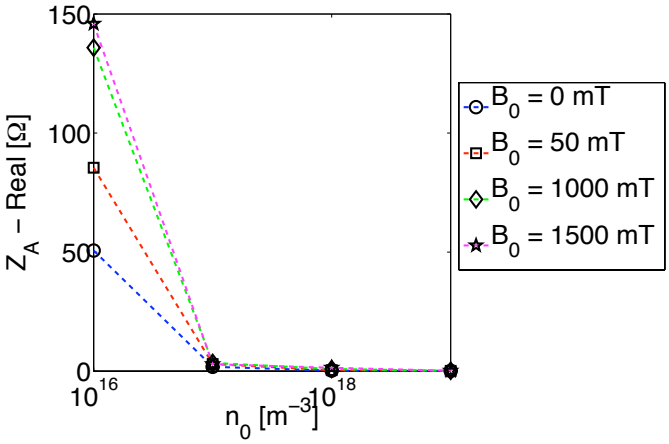

Fig. 6: Input impedance in real part of the GPA of Fig. 2a at $f = 125$ MHz versus the plasma density (n_0) for different values of the external magnetic field.

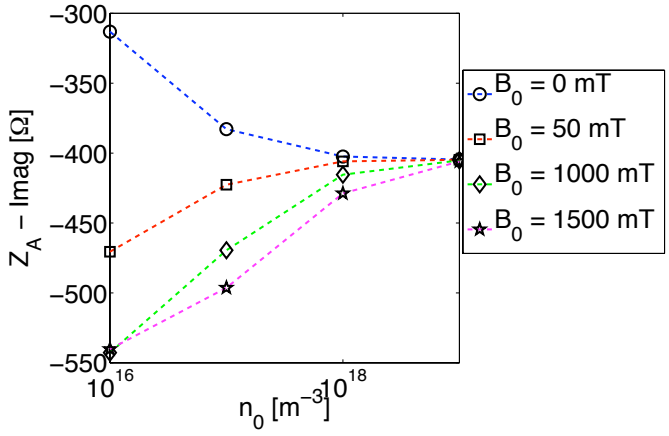

Fig. 7: Input impedance in imaginary part of the GPA of Fig. 2a at $f = 125$ MHz versus the plasma density (n_0) for different values of the external magnetic field.

all along the plasma discharge. In the numerical solution of (6), (7), $\sim$ 20000 and $\sim$ 600 linear div-conforming vector elements have been used in the plasma volume and on the metal parts, respectively. The results are drawn in linear scale for two orthogonal planes (x, z), and (y, z), respectively. We have normalized the RPs to the absolute maximal value.

From Figs. 8, 9 it is evident that the RP can be controlled by adjusting the uniform plasma density; RPs for different density values have dissimilar shapes and magnitude, as attested by the results for $n_0 = 10^{16}$ m^{-3}, in which case the field intensity is much lower than those relevant for other plasma densities. At higher density, i.e., $n_0 = 10^{19}$ m^{-3}, the radiation pattern resembles that of a metallic circular loop of constant current with length approximately the free-space wavelength.

In Figs. 10, 11, we have plotted the real and the imaginary part of the input impedance in real and imaginary part, respectively, as a function of the uniform plasma density. Simulation results indicate that both the real and the imaginary part decrease if the magnetizing field does so.

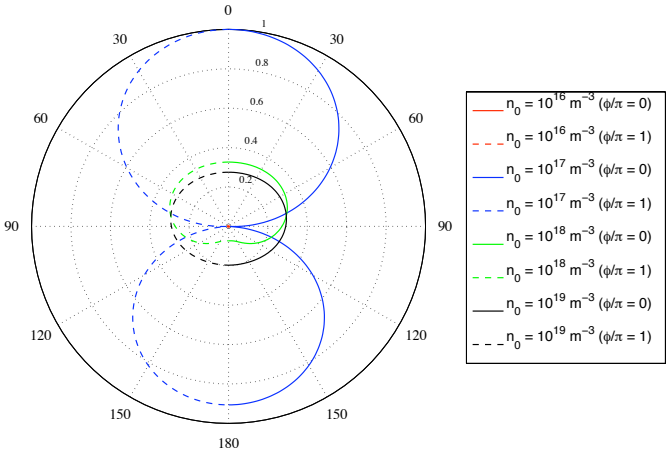

Fig. 8: Radiation pattern of the GPA in Fig. 2b in the (x,z) plane for a non-magnetized plasma driven at $f = 300$ MHz for different values of the plasma density (n_0).

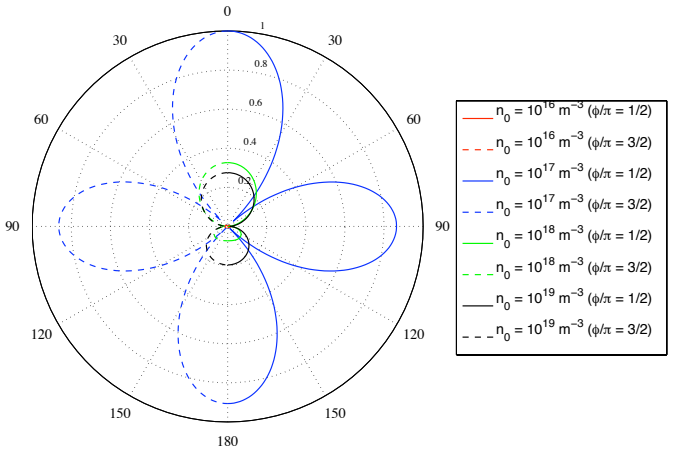

Fig. 9: Radiation pattern of the GPA in Fig. 2b in the (y,z) plane for a non-magnetized plasma driven at $f = 300$ MHz for different values of the plasma density (n_0).

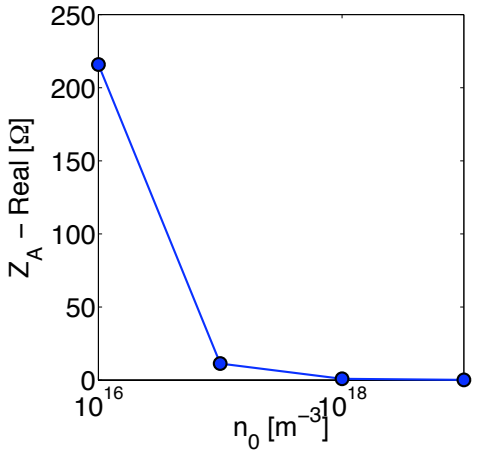

Fig. 10: Input impedance in real part of the GPA of Fig. 2b at $f = 300$ MHz versus the plasma density (n_0).

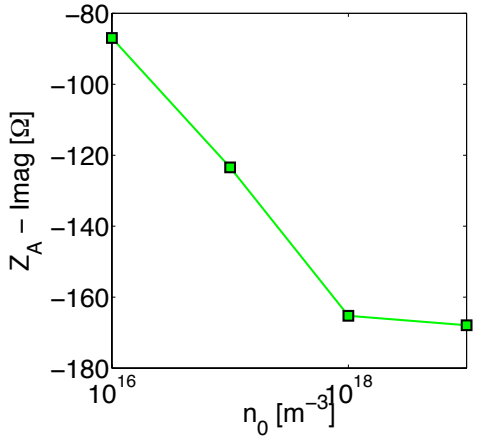

Fig. 11: Input impedance in imaginary part of the GPA of Fig. 2b at $f = 300$ MHz versus the plasma density (n_0) for different values of the external magnetic field.

IV. Conclusion

We have described a numerical approach implemented in the ADAMANT code that allows determining the antenna input impedance and the radiation pattern of reconfigurable plasma antennas, where metal parts provide the excitation of the plasma. Thanks to this approach, complicated GPAs can be analyzed and designed with no limitations in shape.

We have investigated two geometrical configurations, the *plasma dipole* and the *plasma torus*, and analyzed the combined effect of plasma density (n_0) and static magnetic field ($\mathbf{B_0}$) on radiation pattern and input impedance. Due to the geometrical configuration of the plasma torus, no external magneto-static field has been considered in this particular configuration. However, it turns out that plasma discharge parameters can be used to reconfigure both the radiation pattern and field intensity; this suggests that it should be possible to tune the plasma parameters to achieve optimal radiation characteristics.

As regards the GPA behavior as a circuit element, the real part of the antenna impedance decreases as the plasma density increases for both configurations considered.

References

[1] I. Alexeff, T. Anderson *et al.*, "Experimental and theoretical results with plasma antennas," *IEEE Trans. Antennas Propag.*, vol. 32, no. 2, pp. 166–172, 2006.

[2] J. Rayner, A. Whichello, and A. Cheetham, "Physical characteristics of plasma antennas," *IEEE Trans. on Plasma Science*, vol. 32, no. 1, p. 269, 2004.

[3] P. Russo, G. Cerri, and E. Vecchioni, "Self-consistent model for the characterization of plasma ignition by propagation of an electromagnetic wave to be used for plasma antennas design," *IET Microwaves, Antennas & Propagation*, vol. 4, no. 12, pp. 2256–2264, March 2010.

[4] D. Melazzi, V. Lancellotti, "ADAMANT: A Surface and Volume Integral-Equation Solver for the Analysis and Design of Helicon Plasma Sources," *Comp. Phys. Comm.*, *under review*